



HAL
open science

Rotational excitation of 36 ArH^+ by He at low temperature

Cheikh T Bop, Kamel Hammami, Aliou Niane, Ndeye Arame Boye Faye, N Jaïdane

► **To cite this version:**

Cheikh T Bop, Kamel Hammami, Aliou Niane, Ndeye Arame Boye Faye, N Jaïdane. Rotational excitation of 36 ArH^+ by He at low temperature. Monthly Notices of the Royal Astronomical Society, 2016, 465 (1), pp.1137-1143. hal-03078739

HAL Id: hal-03078739

<https://hal.science/hal-03078739>

Submitted on 13 Oct 2021

HAL is a multi-disciplinary open access archive for the deposit and dissemination of scientific research documents, whether they are published or not. The documents may come from teaching and research institutions in France or abroad, or from public or private research centers.

L'archive ouverte pluridisciplinaire **HAL**, est destinée au dépôt et à la diffusion de documents scientifiques de niveau recherche, publiés ou non, émanant des établissements d'enseignement et de recherche français ou étrangers, des laboratoires publics ou privés.

Rotational excitation of $^{36}\text{ArH}^+$ by He at low temperature

Cheikh T. Bop,^{1*} K. Hammami,^{2*} A. Niane,¹ N. A. B. Faye¹ and N. Jaïdane²

¹Laboratory of Atoms Lasers, Department of Physics, Faculty of Science and Techniques, University Cheikh Anta Diop, Dakar 5005, Senegal

²Laboratory of Atomic Molecular Spectroscopy and Applications, Department of Physics, Faculty of Science, University Tunis El Manar, Campus Universities, 1060 Tunis, Tunisia

Accepted 2016 October 28. Received 2016 October 24; in original form 2016 August 30

ABSTRACT

In this paper, we focus on the determination of the rotational excitation rate coefficients of the first observed molecule containing noble gas $^{36}\text{ArH}^+$ isotope by He. Hence, we present the first potential energy surface (PES) of $\text{ArH}^+ - \text{He}$ van der Waals system. The interaction PES of the $\text{ArH}^+(\text{X}^1\Sigma^+) - \text{He}(^1\text{S})$ complex is calculated by the ab initio explicitly correlated coupled cluster with single, double, and perturbative triple excitation (CCSD(T)-F12) method in connection with the augmented correlation consistent triple zeta Gaussian basis (aug-cc-pVTZ). The interaction potential presents two global minima of 708.00 and 172.98 cm^{-1} below the $\text{ArH}^+(\text{X}^1\Sigma^+) - \text{He}(^1\text{S})$ dissociation limit. Using the PES obtained, we have computed integral inelastic cross-sections in the close-coupling approach among the first 11 rotational levels of ArH^+ for energies up to 2500 cm^{-1} . Downward rate coefficients were determined at low temperature ($T \leq 300$ K). It is expected that the data worked out in this study may be beneficial for further astrophysical investigations as well as laboratory experiments.

Key words: molecular data – molecular processes – ISM: abundances – ISM: molecules – ISM: supernova remnants.

1 INTRODUCTION

The arrival of the *Herschel Space Observatory* in 2009 has offered a wide expansion of the capabilities of early space missions. It provided a powerful probe of the far-infrared and submillimeter spectral regions (Pilbratt 2010). Therefore, the first cationic hydrides H_2Cl^+ (Lis et al. 2010), H_2O^+ (Ossenkopf et al. 2010), and HCl^+ (De Luca et al. 2012) were detected in the interstellar medium (ISM) with *Herschel*. These detections and molecular modelling are crucial for investigating the physical and chemical conditions of interstellar clouds. Therefore, accurate information on the collisional processes occurring in the ISM are required. To satisfy this requirement, it is recommended to treat the collisional dynamics with the best astrophysical precision (Roueff & Lique 2013). An important amount of theoretical as well as experimental efforts have been devoted in the last four decades to study the collision-inducing rotational energy transfer. The rate coefficients of interstellar molecules in collision with the most abundant species, H_2 , H, and He, are of great astrophysical importance (Dubernet et al. 2009; Lique et al. 2009, 2010; Najar et al. 2009; Nkem et al. 2009; Sarrasin et al. 2010; Gotoum et al. 2011, 2012; Ajili & Hammami 2013; Niane et al. 2014).

The most abundant species in the ISM, H_2 ($j = 0$), is isoelectronic to helium. It is common for astronomers to evaluate the rate coefficients for the collisions with para- H_2 ($j = 0$) from those worked out using He (Schöier et al. 2005). For charged species, Monteiro

(1985) has shown that it is desirable to use a scaled factor between 2 and 4 to approximate rate coefficients of collision with para- H_2 using the data obtained from collision with He.

$^{36}\text{ArH}^+$ was detected for the first in the ISM towards the Crab Nebula (Barlow et al. 2013), showing spatially extended emission in the $1 \rightarrow 0$ and $2 \rightarrow 1$ rotational lines. Argon-36 was expected to be originated from explosive nucleosynthesis in massive stars during core-collapse supernova events until its detection in the Crab Nebula. The product of such a supernova event, confirms this expectation. More recently, Schilke et al. (2014) and Müller et al. (2015) reported on their early detections of the $\text{ArH}^+ 1 \rightarrow 0$ transition in emission, respectively, towards six continuum sources [viz. SgrB2(M), SgrB2(N), G34.26+0.15, W31C (G10.60–0.39), W49(N), and W51e] and PKS 1830–211. These last observations, on one hand, let us expect that the isotopic ration evolution depending on the redshift may be important to confine nucleosynthetic scenarios that occurred in the early Universe. On the other hand, argonium is demonstrated to be a suitable tracer of gas with a very low fractional H_2 abundance (10^{-4} to 10^{-3}) using a chemical model for diffuse molecular clouds. The abundances in our planet of ^{36}Ar , ^{38}Ar , and ^{40}Ar are about 0.33 per cent, 0.06 per cent, and 99.60 per cent (Nier 1950; Lee et al. 2006), respectively. Indeed, many experimental and theoretical studies on the argonium chemistry reported in the past concerned the $^{40}\text{ArH}^+$ isotope (Song et al. 2003; Mitchel et al. 2005; Rey et al. 2006; Aleksey, Heinz & Buenker 2007; Kreckel et al. 2008; Méndez, Tanarro & Herrero 2010; Liu, Liu & Zhang 2011; Mensah et al. 2012; Hu et al. 2013; Sode, Swwarz-Selinger & Jacob 2013a,b) and then few

* E-mail: aacatbop@gmail.com (CTB); hammami283@gmail.com (KH)

data are available for $^{36}\text{ArH}^+$, and even less for $^{38}\text{ArH}^+$. However, in the Sun, 84.6 per cent of argon is ^{36}Ar (Lodders 2008) and in giant planets $^{36}\text{Ar}/^{40}\text{Ar}$ is 8600 (Cameron 1973). The recent discoveries of $^{36}\text{ArH}^+$ and $^{38}\text{ArH}^+$ in different chemical environments in the ISM have revived the interest in the mechanisms for the production and destruction of these ions (Cueto et al. 2014; Redondón et al. 2014; Roueff, Alekseyev & Le Bourlot 2014; Theis, Morgan & Fortenberry 2015; Novak et al. 2016). These investigations summarize interstellar argonium mechanisms into the following reactions:



The main excitation mechanism for the observed ArH^+ emission lines (Barlow et al. 2013) is likely to be collisions with either electrons or H_2 molecules. Loh et al. (2012) reported that the gas abundance of hydrogen in any form in the molecular region of the Crab Nebula is about 10 times greater than the electron one, in addition an intensity ratio $I(\text{H}_2\ 2.12\ \mu\text{m})/I(\text{H I Br}\gamma)$ of 10 was observed. Thus, argonium is preferentially excited by molecular hydrogen (see Section 3 for further discussions on ArH^+ collisional partner). In the paper of Barlow et al. (2013), $\text{SiH}^+ + \text{He}$ collisional de-excitation rates are used in place of those of the title molecule in collision with H_2 to estimate corresponding H_2 critical density. This approximation and the ArH^+ mechanism of destruction (equation 3) point out the necessity to perform rate coefficients of the rotational collision between $^{36}\text{ArH}^+$ and He.

The rotational constants for the three argonium isotopes differ by $0.01\ \text{cm}^{-1}$ (Hamilton, Faure & Tennyson 2016). Thus, this work takes an interest in studying the rotational (de-)excitation rate coefficients of $^{36}\text{ArH}^+$ (the most abundant isotope in the ISM) in collision with He via quantum mechanical treatment. The data worked out are useful for both observed isotopes. Hence, we performed a new accurate ab initio two-dimensional potential energy surface (PES) to compute close-coupling (CC) cross-sections among the first 11 rotational levels for total energy up to $2500\ \text{cm}^{-1}$. The collisional rate coefficients are obtained by averaging these cross-sections over a Maxwell–Boltzmann velocity distribution at low temperatures ranging from 2 to 300 K.

This paper is organized as follows: Section 2 describes the ab initio PES computational details. The results of dynamic calculation are presented and discussed in Section 3. Concluding remarks are detailed in Section 4.

2 POTENTIAL ENERGY SURFACE

Due to the fact that we are interested in studying low-temperature collisions, the vibrational excitation is expected to be negligible. To perform our calculations, we describe in Fig. 1 the van der Waals $\text{ArH}^+ - \text{He}$ complex by Jacobi coordinates (r, R, θ) . The internuclear distance of ArH^+ is held fixed at its experimental equilibrium geometry $r = r_e = 1.292\ \text{\AA}$. The use of this value is justified because it differs slightly ($0.002\ \text{\AA}$) to the averaged r -distance ($1.290\ \text{\AA}$) at the fundamental vibrational level ($v = 0$). The validity of such approximation has been proven by Murdachaew et al. (2004), showing that the $\text{HCl} - \text{He}$ PES depends weakly to the HCl bond length. Thus, we have used the rigid rotor approximation, although Kalugina, Lique & Marinakis (2014) have proposed that vibrationally averaged PES should be used instead of pure two-dimensional PES for studying

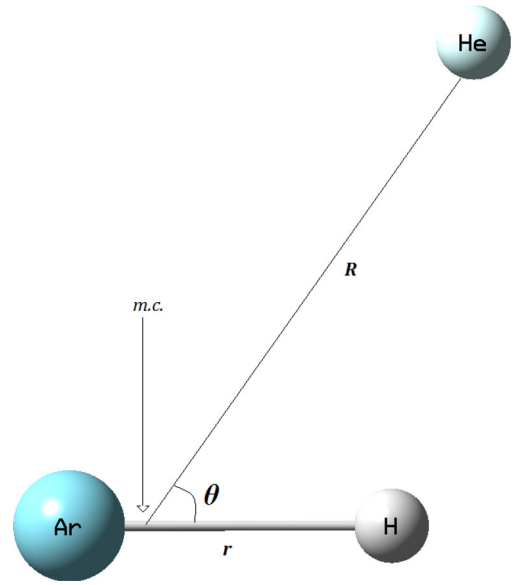


Figure 1. Definition of the coordinate system of Jacobi for the $\text{AH}^+ - \text{He}$ complex.

the excitation of diatomic hydrides by He. R represents the distance between the mass centre (m.c.) of ArH^+ and He, and θ is the angle that forms the two distance vectors. $\theta = 0^\circ$ corresponds to the linear geometry $\text{ArH}^+ \dots \text{He}$. We varied the distance R from 2.5 to $10\ a_0$ by step of $0.25\ a_0$ and then between 10 and $20\ a_0$ by step of $1\ a_0$. θ was varied between 0° and 180° with a regular step of 10° . All these configurations generated 779 ab initio geometries that were treated in the C_s symmetry group.

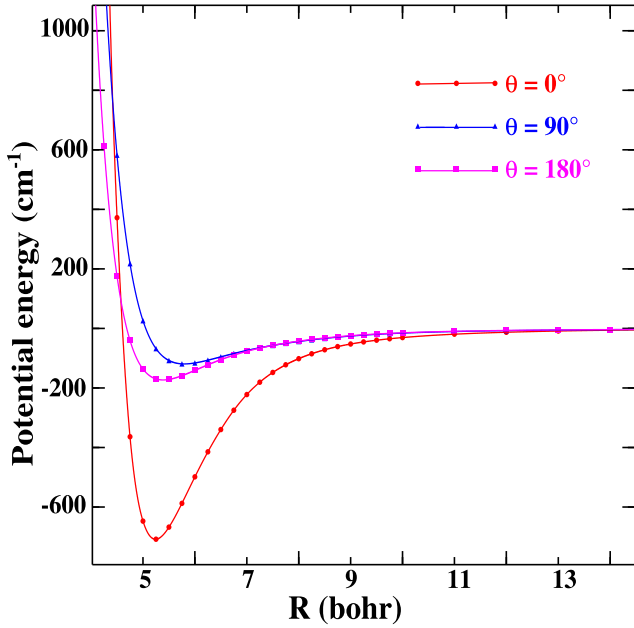
The interaction energy of the $\text{ArH}^+ - \text{He}$ system is calculated using the explicitly correlated coupled cluster with single, double, and perturbative triple excitation (CCSD(T)-F12) method (Knizia, Adler & Werner 2009) as implemented in the MOLPRO package (Werner et al. 2010). Because the weight of the dominant configuration ($1a'^2 2a'^2 3a'^2 4a'^2 1a''^2 5a''^2 6a''^2 7a''^2 8a''^2 2a''^2$) of the fundamental state is greater than 99.0 per cent for all geometries, the use of the monoconfigurational standard coupled cluster approach is suitable. Within the above standard computations, the atoms are described using aug-cc-pVTZ basis set (Dunning 1989; Kendall, Dunning & Harrison 1992). For explicitly correlated computations, we followed the tactics of Nasri et al. (2015) using the above basis set and also the corresponding auxiliary ones and density fitting functions (Klopper 2001; Weigend, Kohn & Hattig 2002; i.e. the default CABS (OptRI) of Peterson, Adler & Werner 2008 as implemented in MOLPRO).

To the basis sets is added a set of bond functions ($3s3p2d2f1g$) defined by Cybulski & Toczylowski (1999) and placed at mid-distance between the mass centre of the ArH^+ molecule and He atom. These bond functions have proven to be very efficient for the correct description of the intersystem correlation (Miller et al. 1988; Niane et al. 2012). The basis set superposition errors were corrected in all geometries using the counterpoise procedure of Boys & Bernardi (1970).

The total energies obtained using both approximations (CCSD(T)-F12a and CCSD(T)-F12b) are very close. Hereafter, we will consider the CCSD(T)-F12a results (denoted as CCSD(T)-F12). To force the potential calculated with this method to decay to zero, it was uniformly shifted by the corresponding asymptotic value ($R = 100\ a_0$). Table 1 presents a comparison of the interaction

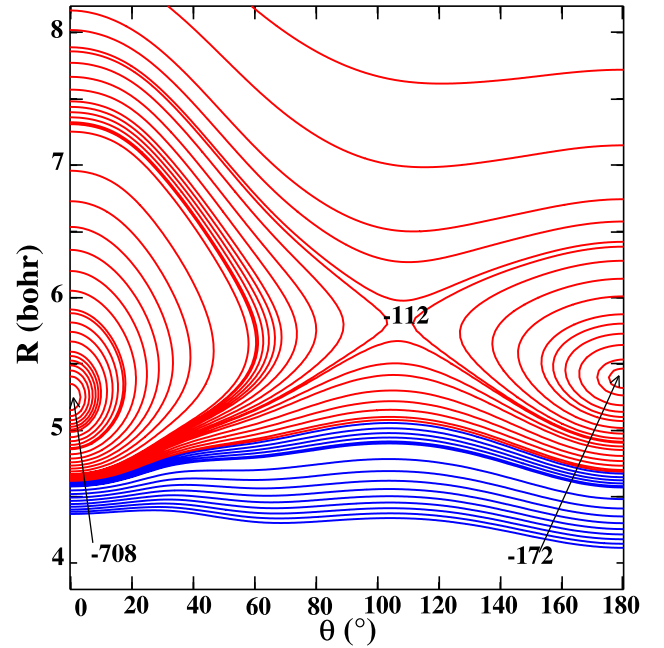
Table 1. PES (in units of cm^{-1}) of the ArH^+ –He system for the linear arrangement ($\theta = 0^\circ$) computed at different levels of theory as a function of the distance R (a_0).

R	CCSD(T)/ aVQZ	CCSD(T)/ aV5Z	CCSD(T)/ CBS	CCSD(T)-F12/ VTZ	CCSD(T)-F12/ VQZ	CCSD(T)-F12/ aVTZ	CCSD(T)-F12/ aVQZ
5.15	−694.309	−699.513	−707.659	−700.108	−699.174	−700.904	−701.819
5.20	−700.528	−705.084	−712.918	−705.485	−704.611	−706.765	−707.260
5.25	−702.051	−706.039	−713.523	−706.255	−705.440	−708.001	−708.053
5.30	−699.590	−703.089	−710.186	−703.127	−702.371	−705.350	−704.938
5.35	−693.775	−696.857	−703.569	−696.694	−696.007	−699.454	−698.542


Figure 2. Cuts of the PES as a function of the distance R for three values of θ : 0° , 90° , and 180° .

potential computed at different levels of theory as a function of the distance R around the well depth. The first point is that the position of the global minimum has not changed depending on the level of theory. The values calculated with the CCSD(T)-F12 method using the augmented basis sets (aVTZ and aVQZ) are slightly deeper than those obtained with VTZ and VQZ, respectively. For each type of basis set (VXZ and aVXZ, X = T, Q), the CCSD(T)-F12 provides similar values of potential (i.e. the potential varies slowly with the expansion of the basis from TZ to QZ). Moreover referring to the standard CCSD(T) with the complete basis set (CBS), CCSD(T)-F12/aVTZ level of theory is more close to the reference than CCSD(T)/aV5Z one. For $R = 5.25 a_0$, the relative errors calculated with these methods are 0.78 and 1.06 per cent, respectively. In addition to the analysis of Table 1, Nasri et al. (2015) proved that the CCSD(T)-F12/aVTZ level of theory is accurate enough to describe correctly the regions of the van der Waals intermolecular interactions, which are sensitive to electron correlation.

Fig. 2 presents three cuts of the PES : $V(r_e, R_{\text{He}\dots\text{ArH}^+}, \theta = 180^\circ)$, $V(r_e, R_{\text{ArH}^+\perp\text{He}}, \theta = 90^\circ)$ and $V(r_e, R_{\text{ArH}^+\dots\text{He}}, \theta = 0^\circ)$. $R_{\text{ArH}^+\dots\text{He}}$ represents R for a linear approach of He towards H, $R_{\text{ArH}^+\perp\text{He}}$ is the value of R in the T-shape geometry and $R_{\text{He}\dots\text{ArH}^+}$ represents R for an approach of He towards Ar. For $\theta = 0^\circ$ ($\theta = 180^\circ$), the minimum is located at $R_{\text{ArH}^+\dots\text{He}} = 5.25 a_0$ ($R_{\text{He}\dots\text{ArH}^+} = 5.40 a_0$) with a well depth of 708.00 cm^{-1} (172.98 cm^{-1}) and for the T-shape geometry the minimum occurs at 118.95 cm^{-1} at the


Figure 3. Contour plot of the PES (in cm^{-1}) of $\text{ArH}^+(\text{X}^1\Sigma^+) - \text{He}(^1\text{S})$ as a function of R and θ ($r_e = 1.929 a_0$). The zero of energy corresponds to the ArH^+ –He asymptote.

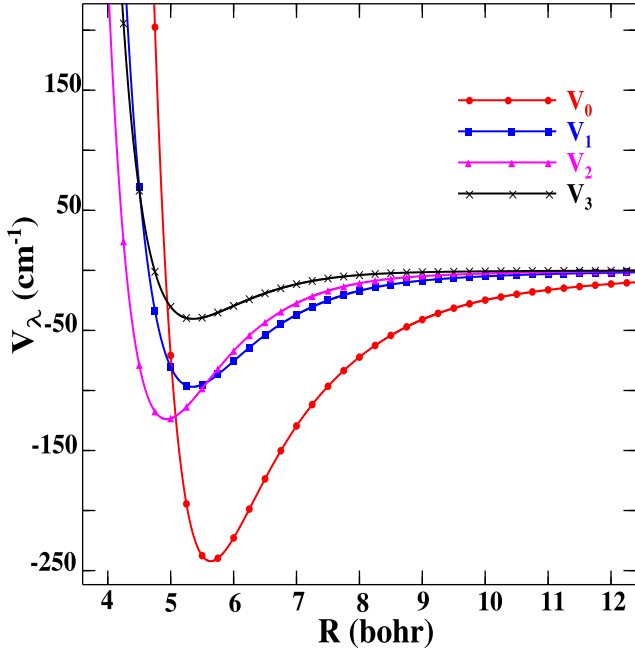
coordinates $R_{\text{ArH}^+\perp\text{He}} = 5.75 a_0$. These values are obtained after refinement using the cubic splines interpolation. Fig. 3 displays the contours plot of the ArH^+ –He PES as a function of R and θ . It is clear from figure that the interaction potential presents two global minima corresponding to the linear He orientations. The deepest, which occurs towards the H side at the coordinates mentioned above, is the one of 708.00 cm^{-1} .

The two protonated atoms SiH^+ and ArH^+ were identified into the diffuse interstellar clouds and the collisional de-excitation rate coefficients of $\text{SiH}^+ + \text{He}$ were used in place of those of $\text{ArH}^+ + \text{H}_2$ (Barlow et al. 2013) to estimate the critical density of H_2 . As rate coefficients are derived from PESs, it is relevant to compare the PESs of the SiH^+ –He and ArH^+ –He systems to verify the validity of the above estimation.

Table 2 compares the global minima of the complexes mentioned above. The SiH^+ –He system owns a global minimum of 308.21 cm^{-1} at the coordinates $R = 5.0 a_0$ and $\theta = 78^\circ$ (close to the T-shape geometry; Nkem et al. 2009), while for the ArH^+ –He complex we have two global minima which occur at the linear He orientations. The potential well of 708.00 cm^{-1} (almost twice deeper than the SiH^+ –He one) occurs at $5.25 a_0$ and 0° . As one can see these two PESs hardly defer by shape and well depth. Moreover, the charge distribution into atoms of both molecular ions calculated

Table 2. Global minima of the $\text{ArH}^+\text{-He}$ and $\text{SiH}^+\text{-He}$ PESs (in units of cm^{-1}).

Coordinates		This work	Nkem et al. (2009)
R (a_0)	θ ($^\circ$)	$\text{ArH}^+\text{-He}$	$\text{SiH}^+\text{-He}$
5.25	0	708.00	–
5.40	180	172.98	–
5.00	78	–	308.21

**Figure 4.** Radial coefficients (V_λ in cm^{-1}) expansions of the interaction PES ($\lambda = 0, 1, 2, 3$) as a function of the distance R .

at the CCSD(T)-F12/aug-cc-pVTZ level of theory reveals that for ArH^+ the positive charge is almost allocated in equal proportions into atoms (+0.48 and +0.52 for Ar and H, respectively) while it is completely shifted to the silicon one for SiH^+ (+1.12 and -0.12 for Si and H, respectively). The differences into the electronic behaviour of these systems let us expect that the use of the SiH^+ rate coefficients instead of the ArH^+ ones is not accurate.

To enable the basic input required by the MOLSCAT package (Huston & Green 1994) used in dynamic calculations, we have fitted the ab initio points on the basis of Legendre polynomial functions, described in detail by Hammami et al. (2008) obtained in the most convenient analytical form:

$$V(R, \theta) = \sum_{\lambda=0}^{\lambda_{\max}} V_\lambda(R) P_\lambda(\cos \theta). \quad (4)$$

From the PES containing 19 ab initio values of λ , we are able to include terms up to $\lambda_{\max} = 18$. Fig. 4 displays the dependence on R of the first $V_\lambda(R)$ components. We observe that the largest (in magnitude) of the anisotropic terms ($\lambda > 0$) corresponds to $\lambda = 1$. From all the forgoing results, we deduced that our scattering calculations may be carried out faithfully for R starting from $2.5 a_0$. This value gives sufficiently repulsive potential (for magnitude ranking between 10^4 and 10^6) for all geometries. During the scattering calculations, an extrapolation was performed to obtain $V_\lambda(R)$ at the values of R less (and greater) than $2.5 a_0$ ($20 a_0$) with the POTENL routine as it is implemented in the MOLSCAT code. For $R > 20 a_0$, the

Table 3. MOLSCAT parameters used in this work.

$B_e = 10.27267 \text{ cm}^{-1} a$	$J_{\max} = 13, 15, 17$	STEPS = 20, 10
$D_e = 6.189765 \times 10^{-4} \text{ cm}^{-1} a$	$R_{\min} = 2 a_0$	DTOL = 0.01 \AA^2
$\mu = 3.61164 \text{ au}$	$R_{\max} = 40 a_0$	OTOL = 0.001 \AA^2

Note. ^aBrown et al. (1988).

$V_\lambda(R)$ parameters are extrapolated by inverse exponent expansion as follows:

$$V_\lambda(R) = \frac{C_\lambda}{R^{\eta_\lambda}}. \quad (5)$$

The routine considers the latest $V_\lambda(R)$ values to calculate the η_λ and C_λ coefficients for each value of λ . For example, it gives $\eta_{(\lambda=0)} = 4.251$, $\eta_{(\lambda=1)} = 5.058$, and $\eta_{(\lambda=2)} = 6.041$. These values are in good agreement with the expressions of the long-range interaction potential between positively charged molecule and structureless atom (Buckingham 1967).

3 DYNAMICAL CALCULATIONS

3.1 Cross-sections

This work focuses on the study of the rotational (de-)excitation of $^{36}\text{ArH}^+$ in collision with He and use the results as a template for collisions with H_2 . Therefore, as helium is a closed shell atom with two electrons, it can be used as a model for para- H_2 (Schöier et al. 2005; Lique et al. 2008; Gómez-Carrasco et al. 2014). Despite the similar results on ionic hydrides (HCO^+) excitations with He (Monteiro 1985) and para- H_2 (Flower 1999), the use of He as template of H_2 is questionable for the excitation of molecular hydrides (Lanza et al. 2014). Nevertheless, the data worked out in this paper will enable rough approximate of the magnitude rank of the interstellar ArH^+ collisional processes, which are of extreme importance for modelling the excitation and abundance of argonium in the ISM.

The collision rates were calculated at low temperature ($T \leq 300 \text{ K}$) for J up to 10 and the cross-sections were performed for total energies ranging from 10.3 to 2500 cm^{-1} . J is the rotational momentum of ArH^+ molecule. We calculated the rotational levels of the argonium using the usual expansion with the constants of rotation B_e and centrifugal distortion D_e represented in Table 3. The cross-sections are computed using the quantum mechanical CC approach of Arthur & Dalgarno (1960) implemented in the MOLSCAT code: for $E < 100 \text{ cm}^{-1}$ the energy step was set to 0.1 cm^{-1} ; for $100 \leq E < 150 \text{ cm}^{-1}$ to 0.2 cm^{-1} ; for $150 \leq E < 200 \text{ cm}^{-1}$ to 0.5 cm^{-1} ; for $200 \leq E < 500 \text{ cm}^{-1}$ to 1 cm^{-1} ; for $500 \leq E < 1000 \text{ cm}^{-1}$ to 5 cm^{-1} , and for $1000 \leq E < 2500 \text{ cm}^{-1}$ to 20 cm^{-1} . The STEPS parameter that determines the integration step was set to 20 for $E < 100 \text{ cm}^{-1}$ and 10 for the other energy values. In addition we set $J_{\max} = 13$ for $E < 100 \text{ cm}^{-1}$, $J_{\max} = 16$ for $100 \leq E < 500 \text{ cm}^{-1}$, and $J_{\max} = 17$ for $500 \leq E \leq 2500 \text{ cm}^{-1}$. The above values were selected with convergence tests. The limit value of total angular momentum J_{tot} was fixed large enough for accurate convergence of the cross-sections. The diagonal tolerance (for elastic transitions) was set to 0.01 \AA^2 and the off-diagonal one (for inelastic transitions) to 0.001 \AA^2 . Typically, the maximum value of J_{tot} was 143 at 100 cm^{-1} , 211 at 500 cm^{-1} , and 305 at 2500 cm^{-1} . We have used the propagator of Manolopoulos (1986) to solve the coupled equations.

Fig. 5 presents the collisional excitation cross-sections of $^{36}\text{ArH}^+$ by He as a function of the kinetic energy for transitions involving

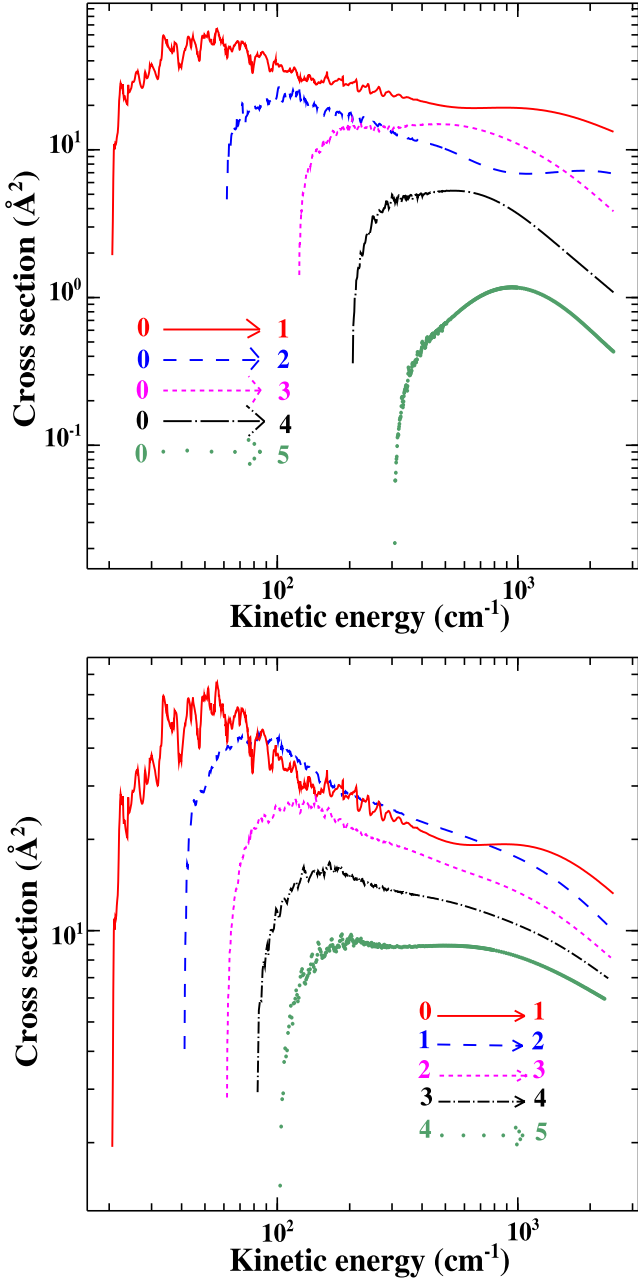


Figure 5. Collisional excitation cross-sections of ³⁶ArH⁺ by He as a function of the kinetic energy for 0 → J' (upper panel) and ΔJ = 1 (lower panel) transitions.

0 → J (upper panel) and ΔJ = 1 (lower panel). These curves present several resonances that occur particularly at low energies. A similar behaviour was observed early in different studies (Smith, Malik & Secres 1979; Christoffel & Bowman 1983; Lique & Spielfiedel 2007). These resonances disappear at high energies. The fine grid used at low energies was necessary for the best description of these resonances. Regarding the propensity rules, we notice that, in the upper panel, the 0 → 1 transition is dominant for all energies and an inversion occurs between the 0 → 2 and 0 → 3 ones from 300 to 1500 cm⁻¹. A global analysis remarks that the odd ΔJ transitions predominate the even ones. Therefore, this propensity rule is owed to the dominance of an odd term V₁ of the radial coefficients

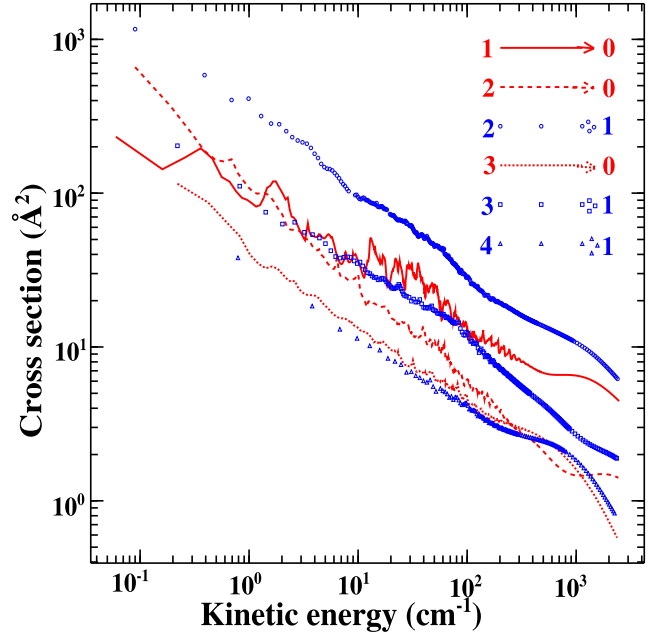


Figure 6. Collisional de-excitation cross-sections of ³⁶ArH⁺ by He as a function of the kinetic energy for J → 0 and J → 1 transitions.

(see Fig. 4). The lower panel shows that the 0 → 1 transition outweighs for high energies ($E > 700$ cm⁻¹).

Fig. 6 displays the collisional de-excitation cross-sections for transitions from J' = 1–3 to 0 and from J' = 2–4 to J = 1. These curves show that the 2 → 1 transition strongly predominates de-excitations for all energies and the 1 → 0 one outweighs the de-excitations to J' = 1 for kinetic energies greater than 10 cm⁻¹. This propensity rule, in favour of transitions with odd Δj, agrees with the reported observed rotational emission lines (1 → 0 and 2 → 1) and will persist in the rate coefficients.

The largest magnitudes of ArH⁺–He and SiH⁺–He (Nkem et al. 2009) excitations differ slightly and are very similar to the data reported in the past for other collisional systems. Nevertheless, the de-excitations computed in this work are very large ($\sim 10^3$ Å²) at low energies but decrease quickly (example the values are ≤ 30 Å² from 100 to 2500 cm⁻¹). Hence, we think these large magnitudes will not influence the rate coefficients.

3.2 Collision rate coefficients

The collision rate coefficients are computed by averaging the calculated cross-sections over the distribution of velocity of Maxwell–Boltzmann:

$$\tau_{J \rightarrow J'}(T) = \left(\frac{8}{\pi \mu \beta} \right)^{1/2} \beta^2 \int_0^\infty E_c \sigma(E_c) e^{-\beta E_c} dE_c \quad (6)$$

$\beta = 1/k_B T$, where T represents the kinetic temperature, k_B the constant of Boltzmann, E_c the kinetic energy [it is the difference between the total energy (E) and the rotational one (E_J), and μ the reduced mass (see Table 3)].

The downward rate coefficients of ArH⁺ in collision with He between the first 11 rotational levels will be reported at the LAMDA¹

¹ <http://home.strw.leidenuniv.nl/moldata>

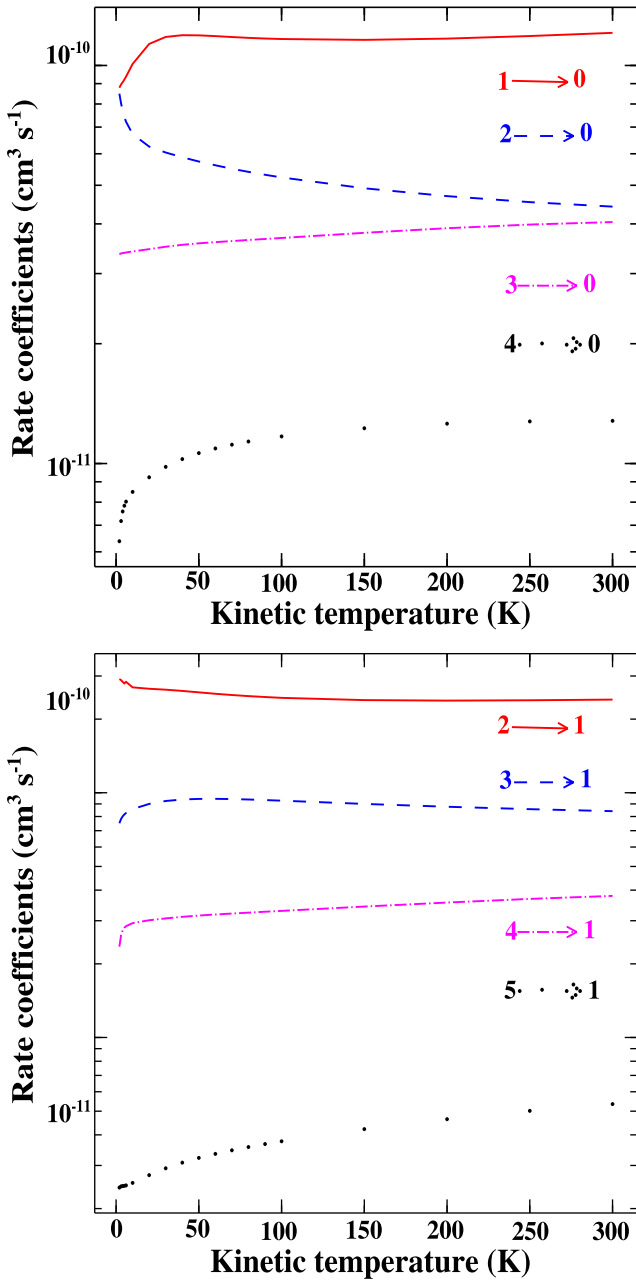


Figure 7. Collisional rate coefficients of $^{36}\text{ArH}^+$ by He as a function of kinetic temperature for transitions $J \rightarrow 0$ (upper panel) and $J \rightarrow 1$ (lower panel).

(Schöier et al. 2005) and BASECOL² (Dubernet et al. 2013) data bases.

We displayed in Fig. 7 the collision rates of ArH^+ –He as a function of the temperature, the upper panel (and the lower one) represents rotational transitions $J \rightarrow 0$ ($J \rightarrow 1$). In this figure, all curves vary slowly with increasing the kinetic temperature. The rate coefficients vary significantly at low temperatures. As it is mentioned above, the transitions involving odd ΔJ values predominate such as $1 \rightarrow 0$ and the $2 \rightarrow 1$ ones, which are already observed in the ISM. Similar propensity rule is observed with the calculations

² <http://basecol.obspm.fr>

of Hamilton et al. (2016) on electron-impact excitation of argonium. Then it is relevant to note that the calculations of Nkem et al. (2009) for SiH^+ –He system, the transition between even ΔJ values predominate. Despite the difference of parities between dominant transitions of the above systems, as we expected, the rate coefficients magnitudes stay the same (10^{-10}). However, the SiH^+ data are not suitable in order to derive the ArH^+ abundance in the ISM because the observed rotational transitions of argonium are approximately three to eight times greater than the corresponding ones of SiH^+ . Furthermore, the averaged ratio ($2 \rightarrow 1$)/($1 \rightarrow 0$) over the temperature grid (up to 300 K) of the collisional rates of ArH^+ with helium (~ 2.4) is about 1.8 times greater than the one obtained with electron (~ 1.3 ; Hamilton et al. 2016). These results could be very useful in order to derive which of these species He, H_2 , and electron is responsible for the rotational emission lines of ArH^+ observed in the Crab Nebula (Barlow et al. 2013).

4 CONCLUSIONS

In this work, a new ab initio PES of the ArH^+ –He complex computed at the CCSD(T)-F12/aug-cc-pVTZ level of theory is presented. This PES is compared to that of Nkem et al. (2009) and we note that their shapes are very different. We have reported CC integral cross-sections involving the lowest rotational levels of $^{36}\text{ArH}^+$ owed by collision with He.

Downward rate coefficients up to $T = 300$ K, were computed by averaging the calculated cross-sections over the distribution of velocity of Maxwell–Boltzmann. A strong propensity towards observed rotational transitions in the ISM is noted for cross-sections and rate coefficients (i.e. transitions with odd Δj). In order to derive argonium abundance in the ISM, the use of the rate coefficients computed in this work instead of SiH^+ ones is more accurate. In fact, the ratios of the averaged rate coefficients $\text{ArH}^+/\text{SiH}^+$ for the $1 \rightarrow 0$ and $2 \rightarrow 1$ transitions are ~ 3.7 and ~ 7.5 , respectively. These results are very useful for astrophysical observations as well as for experiments. The use of our rates for $^{36}\text{ArH}^+$ to interpret observations on all argonium isotopes could have important consequences on the understanding of noble gas molecules chemistry in the ISM.

ACKNOWLEDGEMENTS

This work is supported by the Abdus Salam International Centre for Theoretical Physics, Office of External Activities (ICTP-OEA) under NET45 program.

REFERENCES

- Ajili Y., Hammami K., 2013, *A&A* 556, A82
- Aleksey B., Heinz P. L., Buenker R. J., 2007, *Phys. Chem. Chem. Phys.*, 9, 5088
- Arthurs A. M., Dalgarno A., 1960, *Proc. R. Soc. A*, 256, 540
- Barlow M. J. et al., 2013, *Science*, 342, 1343
- Boys S. F., Bernardi F., 1970, *Mol. Phys.*, 19, 553
- Brown J. M., Jennings D. A., Vanek M., Zink L. R., Evenson K. M., 1988, *J. Mol. Spectrosc.*, 128, 587
- Buckingham A. D., 1967, *Adv. Chem. Phys.* 12, 107
- Cameron A. G. W., 1973, *Space Sci. Rev.*, 14, 392
- Christoffel K. M., Bowman J. M., 1983, *J. Chem. Phys.*, 78, 3952
- Cueto M., Cernicharo J., Barlow M. J., Swinyard B. M., Herrero V. J., Tanarro I., Doménech J. L., 2014, *ApJ*, 783, L5
- Cybulski S. M., Toczyłowski R. R., 1999, *J. Chem. Phys.*, 111, 10520
- De Luca M. et al., 2012, *ApJ*, 751, L37

- Dubernet M.-L., Daniel F., Grosjean A., Lin C. Y., 2009, *A&A*, 497, 911
 Dubernet M.-L. et al., 2013, *A&A*, 553, A50
 Dunning T. H., 1989, *J. Chem. Phys.*, 90, 1007
 Flower D. R., 1999, *MNRAS*, 305, 651
 Gómez-Carrasco S. et al., 2014, *ApJ*, 794, 33
 Gotoum N., Nkem C., Hammami K., Charfadine M. A., Owono Owono L. C., Jaidane N.-E., 2011, *Ap&SS*, 332, 209
 Gotoum N., Hammami K., Owono Owono L. C., Jaidane N.-E., 2012, *Ap&SS*, 337, 553
 Hamilton J. R., Faure A., Tennyson J., 2016, *MNRAS*, 455, 3281
 Hammami K., Owono Owono L. C., Jaidane N., Ben Lakhdar Z., 2008, *J. Mol. Struct.*, 860, 45
 Hu M., Hu W., Liu X., Tan R., Li H., 2013, *J. Chem. Phys.* 138, 174305
 Hutson J. M., Green S., 1994, MOLSCAT computer code, version 14, Collaborative Computational Project No. 6, Science and Engineering Research Council
 Kalugina Y., Lique F., Marinakis S., 2014, *Phys. Chem. Chem. Phys.*, 16, 13500
 Kendall R. A., Dunning T. H., Harrison R. J., 1992, *J. Chem. Phys.* 96, 6796
 Klopper W., 2001, *Mol. Phys.*, 99, 481.
 Knizia G., Adler T. B., Werner H., 2009, *J. Chem. Phys.*, 130, 054104
 Kreckel H., Bing D., Reinhardt S., Petrigiani A., Berg M., Wolf A., 2008, *J. Chem. Phys.*, 129, 164312
 Lanza M., Kalugina Y., Wiesenfeld L., Faure A., Lique F., 2014, *MNRAS*, 443, 3351
 Lee J. Y., Marti K., Severinghaus J. P., Kawamura K., Yoo H.-S., Lee J. B., Kim J. S., 2006, *Geochim. Cosmochim. Acta*, 70, 4507
 Lique F., Spielfiedel A., 2007, *A&A*, 462, 1179
 Lique F., Toboła R., Kłos J., Feautrier N., Spielfiedel A., Vincent L. F. M., Chałasiński G., Alexander M. H., 2008, *A&A*, 478, 567
 Lique F., van der Tak F. F. S., Kłos J., Bulthuis J., Alexander M. H., 2009, *A&A*, 493, 557
 Lique F., Spielfiedel A., Feautrier N., Schneider I. F., Kłos J., Alexander M. H., 2010, *J. Chem. Phys.*, 132, 024303
 Lis D. C. et al., 2010, *A&A*, 521, L9
 Liu X., Liu H., Zhang Q., 2011, *Chem. Phys. Lett.*, 507, 24
 Lodders K., 2008, *ApJ*, 674, 607
 Salomé P., Loh E. D., Baldwin J. A., Ferland G. J., Curtis Z. K., Richardson C. T., Fabian A. C. 2012, *MNRAS*, 421, 789
 Manolopoulos D. E., 1986, *J. Chem. Phys.*, 85, 6425
 Méndez I., Tanarro I., Herrero V. J., 2010, *Phys. Chem. Chem. Phys.*, 12, 4239
 Mensah S. L., Hasseem H. H., Abu-Safe H., Gordon M. H., 2012, *Phys. Plasmas*, 19, 073512
 Miller S., Tennyson J., Follmeg B., Rosmus P., Werner H.-J., 1988, *J. Chem. Phys.*, 89, 2178
 Mitchell J. B. A. et al., 2005, *J. Phys. B: At. Mol. Opt. Phys.*, 38, L175
 Monteiro T., 1985, *MNRAS*, 214, 419
 Müller H. S. P. et al., 2015, *A&A*, 582, L4
 Murdachaew G., Szalewicz K., Jiang H. Bačić Z., 2004, *J. Chem. Phys.*, 121, 11839
 Najar F., Ben Abdallah D., Jaidane N., Ben Lakhdar Z., Chambaud G., Hochlaf M., 2009, *J. Chem. Phys.*, 130, 204305
 Nasri S., Ajili Y., Jaidane N.-E., Kalugina Y. N., Halvick P., Stoecklin T., Hochlaf M., 2015, *J. Chem. Phys.*, 142, 174301
 Niane A., Hammami K., Faye N. A. B., Jaidane N., 2012, *Comput. Theor. Chem.*, 993, 20–25
 Niane A. et al., 2014, SpringerPlus, 3, 188
 Nier A. O., 1950, *Phys. Rev.*, 77, 789
 Nkem C., Hammami K., Manga A., Owono L. O., Jaidane N., Lakhdar Z. B., 2009, *J. Mol. Struct.*, 901, 220
 Novak C. M., Fortenberry R. C., 2016, *J. Mol. Spectrosc.*, 322, 29
 Ossenkopf V. et al., 2010, *A&A*, 518, L111
 Peterson K. A., Adler T. B., Werner H.-J., 2008, *J. Chem. Phys.*, 128, 084102.
 Pilbratt G. L. et al., 2010, *A&A*, 518, L1
 Redondo M. J. et al., 2014, *RSC Adv.*, 4, 62030
 Rey M., Tyuterev V. G., Coxon A. J., Le Roy R. J., 2006, *J. Mol. Spectrosc.*, 238, 260
 Roueff E., Lique F., 2013, *Chem. Rev.*, 113, 8906
 Roueff E., Alekseyev A. B., Le Bourlot J., 2014, *A&A*, 566, A30
 Sarrasin E., Ben Abdallah D., Wernli M., Faure A., Cernicharo J., Lique F., 2010, *MNRAS*, 404, 518
 Schilke P. et al., 2014, *A&A*, 566, A29
 Schöier F. L., van der Tak F. F. S., van Dishoeck E. F., Black J. H., 2005, *A&A*, 432, 369
 Smith L. N., Malik D. J., Secres D., 1979, *J. Chem. Phys.*, 71, 4502
 Sode M., Swwarz-Selinger T., Jacob W., 2013a, *J. Appl. Phys.*, 113, 093304
 Sode M., Swwarz-Selinger T., Jacob W., 2013b, *J. Appl. Phys.*, 114, 063302
 Song J. B., Gislason E. A., 2003, *Chem. Phys.*, 293, 231
 Theis R. A., Morgan W. J., Fortenberry R. C., 2015, *MNRAS*, 446, 195
 Weigend F., Kohn A., Hattig C., 2002, *J. Chem. Phys.* 116, 3175
 Werner H.-J., Molproversion et al., 2010, 1, a package of ab initio programs. Available at <http://www.molpro.net>

This paper has been typeset from a \LaTeX file prepared by the author.